THE ROLE OF THREE-DIMENSIONALITY IN THE DEVELOPMENT OF VORTEX BREAKDOWN IN SWIRLING FLOWS CONFERENCE ON COMPUTATIONAL FLUID DYNAMICS (ECCOMAS CFD 2006)

Dario Amirante, Kai H. Luo

University of Southampton
School of Engineering Sciences, Highfield, Southampton SO17 1BJ, United Kingdom
e-mail: dario@soton.ac.uk

ABSTRACT

Direct numerical simulations of three-dimensional compressible Navier-Stokes equations are conducted using high-order numerical methods in cylindrical coordinates. Aim of the work is to examine the effect of three-dimensionality in the dynamics of vortex breakdown in swirling jets within a specific range of Reynolds numbers. The main elements of vortex breakdown are revealed in our computations, and the interaction between three-dimensional helical instabilities and the axisymmetric process of breakdown is discussed. The results confirm a general tendency of swirling flows to burst into a sequence of bubbles when the Reynolds number is increased. Comparing axisymmetric and fully three-dimensional computations, it's observed the possibility that a single or double helical structure arising in linear regime can work to extract energy from the axisymmetric waves.

1 Introduction

The term vortex breakdown refers to the drastic expansion of the vortex core occurring in swirling flows when the swirl ratio exceeds a threshold value. Although it represents a strongly non-linear phenomenon, many theoretical works [2,9] have provided physical insights based on small perturbations analysis. The leit motiv of all the studies is the capability of a columnar swirling flow to sustain axisymmetric waves.

Lord Kelvin was the first to observe that a vortex tube with uniform axial vorticity behaves as a wave guide for small disturbances. The restoring effect of the wave is generated by a coupling between stretching and tilting of axial vorticity [15]. Squire introduced the concept of criticality in swirling flows [2]: the flow is said to be supercritical when the inertial Kelvin waves are convected downstream from the basic axial flow; if upstream propagation of energy is possible the flow is subcritical. In his view, the breakdwon is the final stage of an amplification process occurring when the flow switches from supercritical to subcritical conditions.

Using a weakly non-linear analysis, Leibovich [6] found that waves of finite amplitude can evolve in a vortex core as a soliton of permanent shape. In his work he indicates the multiple breakdown, *i.e.* the appearence of a second smaller bubble on the axis, as the tail of the soliton. In addition, he explains the well known tendency of the vortex bubble to migrate upstream as the result of a 'positional instability': as the wave grows in amplitude, it becomes faster, and then can penetrate the supercritical region, unaccessible to small perturbations. Thus, in Leibovich's view the key issue of vortex breakdown is the wave dispersion. In figure 1-*a* is reported the dispersion diagram associated to the axisymmetric Kelvin waves for the Rankine vortex. It has been obtained following the standard procedure of normal modes decomposition. For a single axial wave number, there exists an infinite countable sequence of

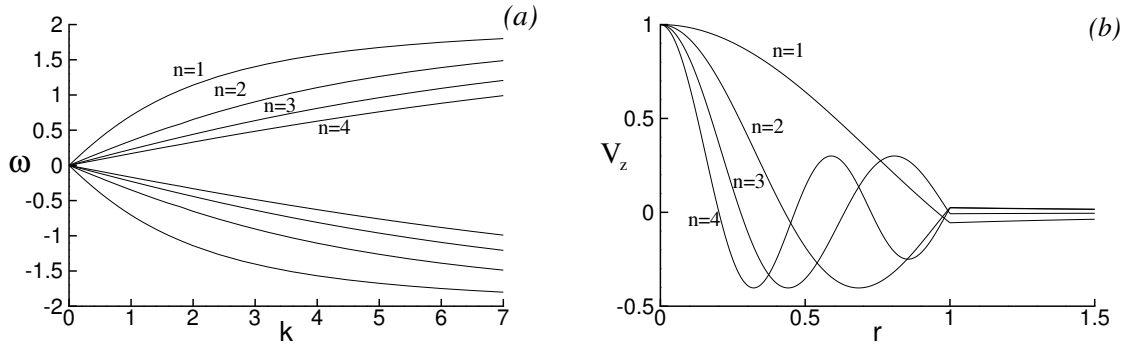

Figure 1: Axisymmetric Kelvin waves sustained by the Rankine vortex. *(a):* Dispersion diagram. *(b):* Normalized eigenfunctions of axial velocity corrisponding to the axial wave number $k = 3/2$.

neutral modes whose temporal frequency lies in the range[1] $-2 < \omega < 2$. Denoting by $\{\}_n$ this sequence, the corresponding eigenfunctions are expressed in terms of Bessel functions of argument nr. Figure 1-*b* reports the eigenfunctions for the first 4 modes. Due to the oscillating nature of Bessel functions, it can be seen that the fastest modes corresponding to a fixed axial wavenumber, are those with less radial structure, and that a lower group velocity competes to the higher wave-numbers k. Now, if the Kelvin waves are responsible for vortex breakdown, it seems reasonable to extend the above dispersion mechanism to the multiple breakdown process: a bigger wave pocket can propagate faster followed behind by slower, smaller pockets. Also, since viscosity is more effective on short wavelengths, the picture provides an explanation for the strong dependence on the Reynolds number found by numerical computations [1] .

An other possibility is to rely multiple breakdown to successive supercritical/subcritical transitions [2,14]. The idea is the following: once the first bubble has developed, the flow field behind it recovers supercritical conditions due to inertial effects, and the subsequent bubble originates when a further transition occurrs in the slowly spatially evolving wake.

In this work, we present a numerical survey on vortex breakdown in swirling jets. Special emphasis is given to the multiple breakdown and to its interaction with the loss of stability to three-dimensional perturbations. Comparing axisymmetric and fully 3D calculations, we have found this coupling mechanism to be dominant when a self sustained global mode contaminates all the domain: since multiple breakdown manifests itself in a series of bubbles sequentially smaller, it turns out that the high wavenumbers are dissipated as soon as the instability occurrs. Nevertheless, we present a higher Reynolds number case in which a certain axial position acts as wave marker for perturbation travelling downstream, leaving unchanged the peculiar structure of multiple breakdown. We believe this case to be representative of the non-linear mechanism discussed by Pier and Huerre [12] for spatially developing wakes.

[1]The time scale is $1/\Omega$, where Ω is the angular velocity of the solid body rotation in the vortex core.

2 Problem formulation and numerical method

The swirling flow under investigation is initially columnar (1D) , with non-dimensional velocity components expressed in cylindrical coordinates (r, θ, z) by:

$$\begin{aligned} V_\theta &= \begin{cases} Sr(2-r^2) & 0 \le r \le 1 \\ S/r & r \ge 1 \end{cases} \\ V_z &= 1 \\ V_r &= 0 \end{aligned} \tag{1}$$

In writing (1) the vortex core radius $\overline{\delta}$ and the uniform axial velocity $\overline{V}_z$ have been used as reference dimensional quantities. The swirl number $S = V_\theta(r=1)/V_z$ is the ratio between the azimuthal velocity at the vortex edge and the uniform axial velocity. It is related to the Rossby number, often referred in the literature, and represents a measure of the intensity of the vortex core. The initial pressure $\overline{p}$ is choosen to balance the centrifugal force, while the density $\overline{\rho}$ is constant through the domain. Thus, assuming $\overline{\rho}$ and $\overline{\rho}\overline{V}_z^2$ as density and pressure reference values, the thermodynamic conditions initially assigned are

$$\begin{aligned} \rho &= 1 \\ T(r) &= 1 + \gamma M_0^2 \int_0^r \frac{V_\theta^2}{s} ds \\ p(r) &= \frac{T(r)}{\gamma M_0^2} \end{aligned} \tag{2}$$

with M_0 the Mach number on the axis.
The unsteady, compressible Navier-Stokes equations are solved in cylindrical coordinates, within a domain of dimension $L_z = 20$, $L_r = 10$ and $0 \le \theta \le 2\pi$. The spatial derivatives in the axial and radial directions are calculated using the 10^{th} order Lele's compact schemes [7]. The method requires the inversion of a penta-diagonal matrix with constant coefficients. Following [4], a lower-upper decomposition is performed in a preliminar stage, and the derivatives are then calculated by simple matrix multiplication. A spectral method employing a base 2 FFT has been used for the periodical direction. The spectral method provides a strightforward way to alleviate the CFL time restriction when the equation are explicitly integrated in time. Indeed, the number of azimuthal modes can be dropped when approaching the axis: a limit point r_0 can be defined such that for $r < r_0$ the number of modes accounted $m_\theta(r)$ is given by

$$m_\theta(r) = \frac{1}{2} N_\theta \frac{r}{r_0} \tag{3}$$

where N_θ is the number of grid points in the azimuthal direction. For the time advancement we used a third order low-storage Runge-Kutta method, and the above strategy has revealed robust and efficient. However, for the higher Reynolds number case presented here, Re=800, resolution requirements has forced us to mantain the number of azimuthal modes nearly constant when moving along the radial direction. For this specific case, to overcome the difficulty of the time step restriction, time integration was performed by a Dual Time Stepping method: equations are discretized in time by a II order backward difference formula

$$\frac{3}{2\Delta t} w_{n+1} - \frac{2}{\Delta t} w_n + \frac{1}{2\Delta t} w_{n-1} = RHS(w_{n+1}) \tag{4}$$

and the solution at level $n+1$ is obtained by integration in a dual variable τ:

$$\frac{dw}{d\tau} = -\frac{3w}{2\Delta t} + RHS(w) - \left[-\frac{2}{\Delta t} w_n + \frac{1}{2\Delta t} w_{n-1} \right] \tag{5}$$

A steady solution of (5) gives the updated physical solution w_{n+1} in (4). The integration in the dual time variable is obtained by a Runge-Kutta Jameson-like scheme [3] with the Local Time Stepping applied to accelerate the convergence.

The boundary conditions are treated with the NSCBC formulation of Poinsot and Lele [13]. To reflect the physical condition of a swirling jet in an open domain, density and velocity are held constant at the inflow according to (1) and (2), while non-reflective boundary conditions are applied at the open sides. For the axis treatment we have adopted the method of O'Sullivan and Breuer [11]: the values in the centre are reconstructed by a Fourier summation

$$\phi(r=0) = \sum_{m=-\frac{N_\theta}{2}}^{N_\theta/2} \hat{\phi}_m(r=0)\ e^{im\theta} \tag{6}$$

with the coefficients calculated using polynomial expansions in the radial direction satisfying specific parity conditions. In particular, for the single valued variables (ρ, V_z, p), it can be seen [8] that

$$\begin{aligned} \hat{\phi}_m(r=0) &= 0 \qquad m \neq 0 \\ \frac{d\hat{\phi}_m}{dr}(r=0) &= 0 \qquad m = 1 \end{aligned} \tag{7}$$

while for the multiple valued variables (V_r, V_θ)

$$\begin{aligned} \hat{\phi}_m(r=0) &= 0 \qquad m \neq \pm 1 \\ \frac{d\hat{\phi}_m}{dr}(r=0) &= 0 \qquad m = \pm 1 \end{aligned} \tag{8}$$

Using (6)-(7) and (8), the values in the center are calculated after performing a modal decomposition of the updated values near the axis. The method of Mohseni and Colonius [10], based on a staggered grid to avoid the singularity, was even tested, but not noticeable differencies were found.

The grid is stretched in the radial direction in order to increase the resolution within the vortex core. The transformation adopted to map the computational variable $0 \leq \eta \leq 1$ into the physical one $0 \leq r \leq L_r$, is given by:

$$r(\eta) = \frac{L_r}{e^a - 1}\left(e^{a\eta} - 1\right) \tag{9}$$

with $a = 0.8$ a stretching factor held constant for all the computations presented. The grid resolution adopted for different Reynolds numbers is reported in table 1.

Re	n_z	n_r	n_θ	r_0
200	256	95	64	0.5
400	256	95	64	0.5
600	320	125	64	0.4
800	320	200	64	0.15

Table 1: Grid resolution for different Reynolds numbers

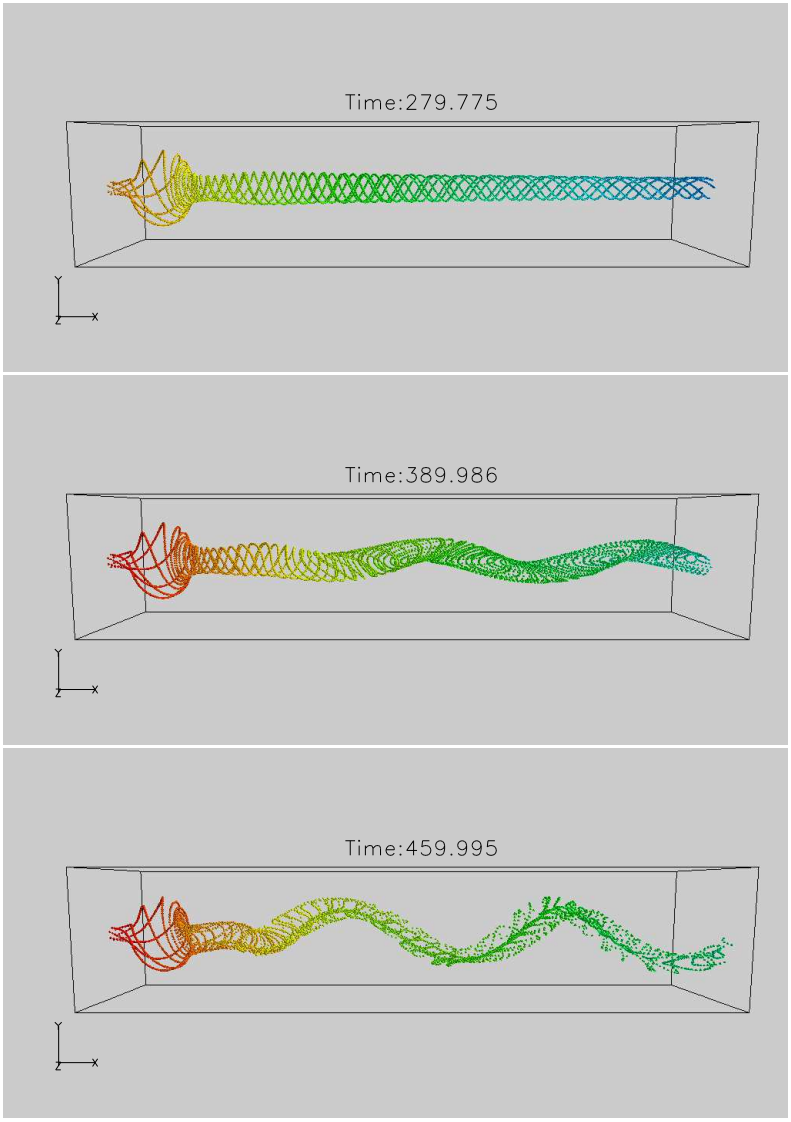

Figure 2: Re=200 S=1.1 case. Temporal evolution of streaklines. Box size: 20x2x2.

3 Results

We study the evolution of the swirling jet defined by equations (1) within the range of Reynolds numbers $200 \leq \text{Re} \leq 800$. In all the computations the Mach number is M_0=0.5. We proceed describing a low Reynolds number case, for which other numerical results are available [14]. This will serve to validate the code and to illustrate the sequence of events characterizing the breakdown process.

3.1 Code validation: Re=200 case

In figure 2 is reported a streaklines visualization for the case Re=200, S=1.1. The streaklines are obtained releasing particles from six positions localized at the inflow boundary (left side), on a circle of radius r=0.1. The particles are coloured according to their emission time. The initial columnar swirling jet

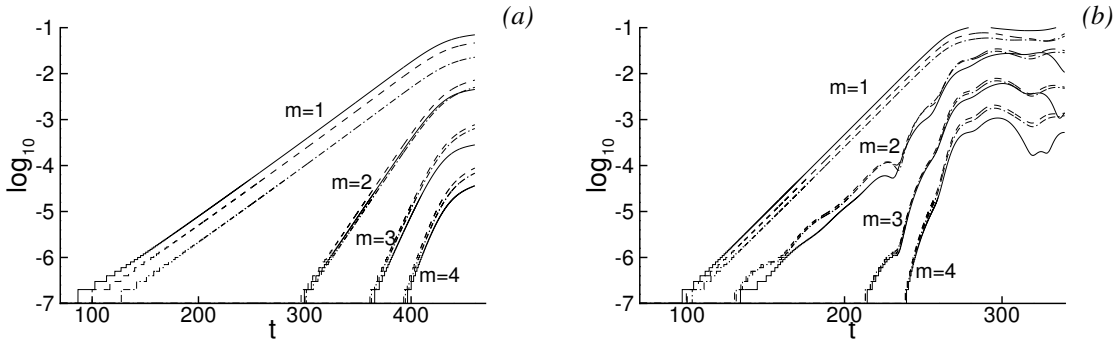

Figure 3: Re=200 case. Temporal evoolution of azimuthal Fourier coefficients for axial velocity (solid), radial velocity (dash), azimuthal velocity (dash-dots). Control station: z=5, r=0.2. *(a):* S=1.1 *(b):* S=1.5.

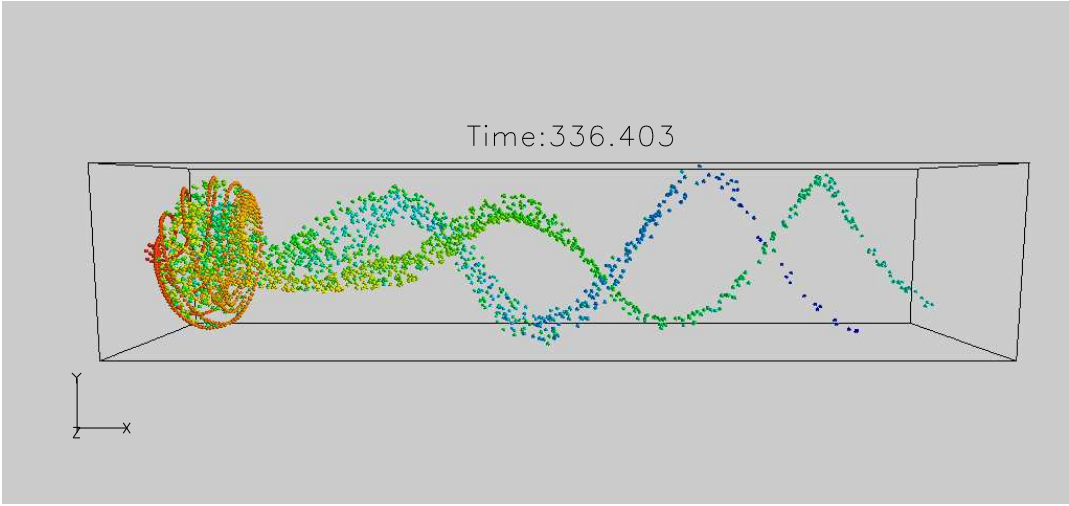

Figure 4: Re=200 S=1.5 case. Streaklines visualization after saturation. Box size: 20x2x2.

rapidly decelerates in the vortex core near the inflow. To satisfy mass conservation the flow expands in the center, and when stagnating conditions are reached a region of recirculating flow (the vortex bubble) is formed. In order to render the computation fully three-dimensional, a small random perturbation in the azimuthal component of velocity was superimposed on the initial conditions. Until the breakdown has fully developed, the flow remains axisymmetric. Then, once the bubble has formed, the wake behind it becomes unstable to the azimuthal disturbance introduced. In figure 3-*a* it is shown the temporal evolution of the first four modes for each velocity component at a control station fixed in the wake of the bubble. The plot is on log scale to highlight the exponential growth rate. The linearly unstable mode is m=1; at Time=300 its amplitude is big enough to render the non-linear interactions not longer negligible, and higher modes start growing in a cascade process. Saturation is reached at approximately Time=420. At this stage, the dominant mode still remains m=1 (ten times bigger than the m=2 amplitude), and the corresponding sreaklines (the 3^{rd} of fig. 2) reveal a stable axisymmetric bubble followed by an helical wake. The helix rotates in the counterclockwise direction if seen from downstream, but it revolves spatially in the clockwise direction. Following the classification of Saffmann [15], it is a *retrograde* mode, *i.e.* in a frame of reference moving with the basic flow, it travels in the negative direction. Same

behaviour has been found in other numerical studies [14], and actually the linear theory confirm the retrograde modes to be the most unstable in swirling wakes [9].
The growth rate for the m=1 mode is calculated by

$$\omega = \frac{1}{t_2 - t_1} \ln \frac{\hat{q}(t_2)}{\hat{q}(t_1)}$$

where $\hat{q}$ is the m=1 Fourier coefficient of any variable, while t_1 and t_2 are different times taken within the linear regime. For this specific case we have found $\omega = 3.8 \cdot 10^{-2}$. Ruith *et al.* [14] found $\omega = 6.63 \cdot 10^{-2}$ with the same velocity profiles but for an incompressible flow. The period of oscillation agree very well, T=6, and the streaklines reveal a very similar spatial structure.

Increasing the swirl number leads to higher growth rates as it can be seen from figure 3-*b* which refers to the S=1.5 case. In addition, the higher modes grow in a less regular way. Higher resolution has not changed this trend which is rather attributed to a competition of effects: for this set of parameters the linearly unstable modes are m=1,2,3. They grow at approximately the same rate until Time=230, then, the growth rate of m=2 and m=3 suddenly increases. Comparing the amplitude values in fig. 3-*a* and fig. 3-*b*, it can be noticed that the transition for the S=1.5 case occurrs when the third mode starts growing in the S=1.1 case. It is therefore suggested that the transition develops when the non-linear poduction of higher modes becomes dominant on the linear higher modes selection. After saturation the amplitude of m=2 becomes comparable with m=1, and the spiral wake switches from a single to a double helix (fig. 4). The disturbance travels into the bubble, where the flow becomes chaotic, and the particles remain trapped before been ejected rotating in clockwise and counterclockwise direction randomly. However, the bubble preserves its original topology of well confined region of recirculating flow.

3.2 Higher Reynolds numbers.

Increasing the Reynolds number to Re=400, the computations reveal a tendency of the flow to manifest multiple breakdowns. In figure 5-*a* we plot the instantaneous streamlines on a meridional plane obtained by axisymmetric calculations. They refer to steady conditions. It can be observed that for S=0.95, the second breakdown is very mild, and located at a considerable distance from the first. Increasing the swirl to S=1.1 renders the second breakdown more pronounced and reduces its distance from the first bubble, which has, in turn, widely increased in size (observe the radius of the recirculating region).

The effect of the Reynolds number can be appreciated comparing figure 5-*a* and 6-*a* which refer to the same level of swirl: it can be noticed that the topology of the flow changes only in the size of the second breakdown. These qualitative results reveal the inviscid nature of the phenomenon and seem to validate the dispersion mechanism described in the introduction. We refer to [1] for a complete discussion on the Reynolds number dependence. What we point out here is that the 3D calculations have temporarily evolved to the same axisymmetric solutions, with the same multiple breakdown configuration. As for the Re=200 case, the flow remains axisymmetric until the breakdown has fully developed. Then, three-dimensional perturbations amplify in the wake and contaminate the whole domain. In figure 5-*b* and 6-*b* are reported the instantaneous streamlines on a single meridional plane after the saturation has been reached. Comparing with the corresponding axisymmetric steady solutions, it can be noticed that the smaller bubbles are completely dissipated, and that for the Re=400 S=1.1 case, even the first bubble appers weakened.

The corresponding streaklines are reported in figure 7. The axial wavenumber of the helix is increased compared to the Re=200 case and is insensitive to the swirl level, while the amplitude of the oscillations is bigger at S=1.1. A further correlated difference is that for the lower swirl case, the first vortex bubble

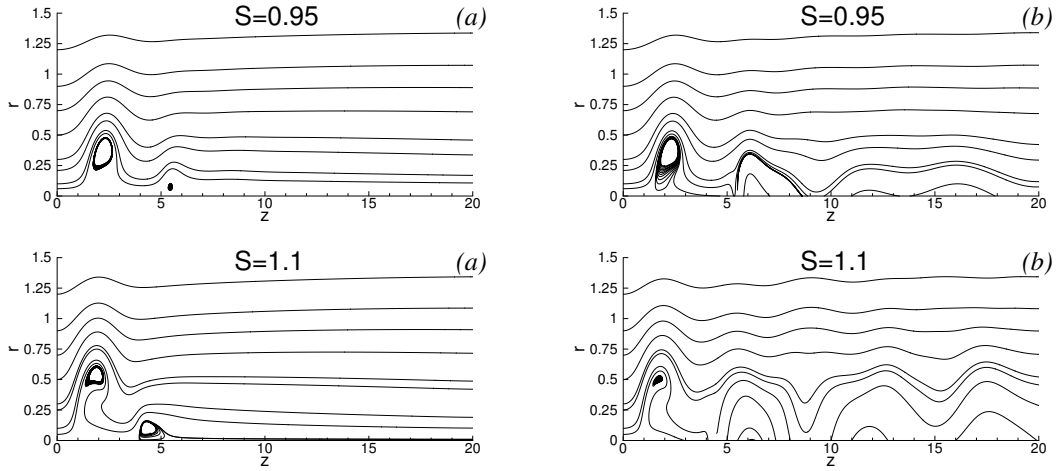

Figure 5: Re=400 case. Streamlines on a meridional planes for different swirl levels. *(a):* steady solutions obtained by axisymmetric calcualtion. *(b)*: three-dimensional calculation after saturation.

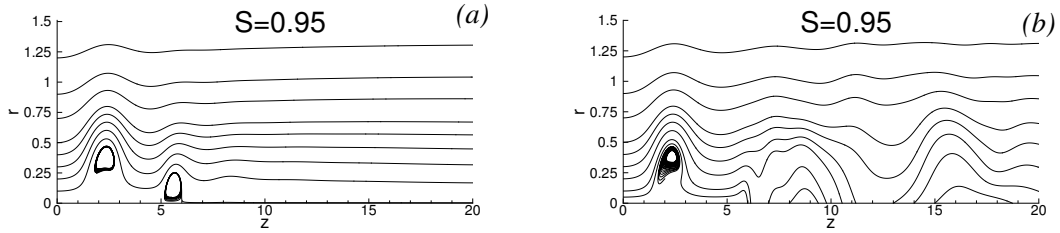

Figure 6: Re=600 case. Streamlines on a meridional planes for different swirl levels. *(a):* steady solutions obtained by axisymmetric calcualtion. *(b)*: three-dimensional calculation after saturation.

remains clearly axisymmetric. The perturbation never propagates upstream of the axial position where the second small bubble had originally developed. A different behaviour is observed for S=1.1. Here, although the second vortex bubble is more pronounced, it is completely swept out and the perturbation moves up to the first bubble. We point out that, at the list for moderate Reynolds numbers, the latter case is representative of the general behaviour observed in most of the simulations, while the former can be considered as a limit case, which, however, resembles very well some breakdown configurations found experimetally [16]

Now we consider the highest Reynolds number under investigation, namely Re=800.
It represents the most interesting case with remarkable qualitative differences. It is instructive to consider the evolution of the flow beginning from the earlier stages when the flow is nearly columnar. From figure 8 it can be seen that the expansion of the vortex core is accompanied by a large upstream excursion. These are the main features of vortex breakdown: a wave growing in amplitude and moving upstream, as discussed in the introduction. It's worth of mentioning that this behaviour can be obtained only if the swirl number is chosen close to the critical point, defined as the minimum level of swirl necessary to breakdown the vortex: fixing an higher swirl leads to a rapid explosion of the vortex core similar to what seen at lower Reynolds numbers. The drawback is that with a moderate swirl the whole dynamics is slower and the time needed increases proportionally to the Reynolds number. Furthermore, the combination high Reynolds - moderate swirl leads to a strong domain dependence. Consequently, the computational effort necessary to highlight the wave like connotations of vortex breakdown, is very

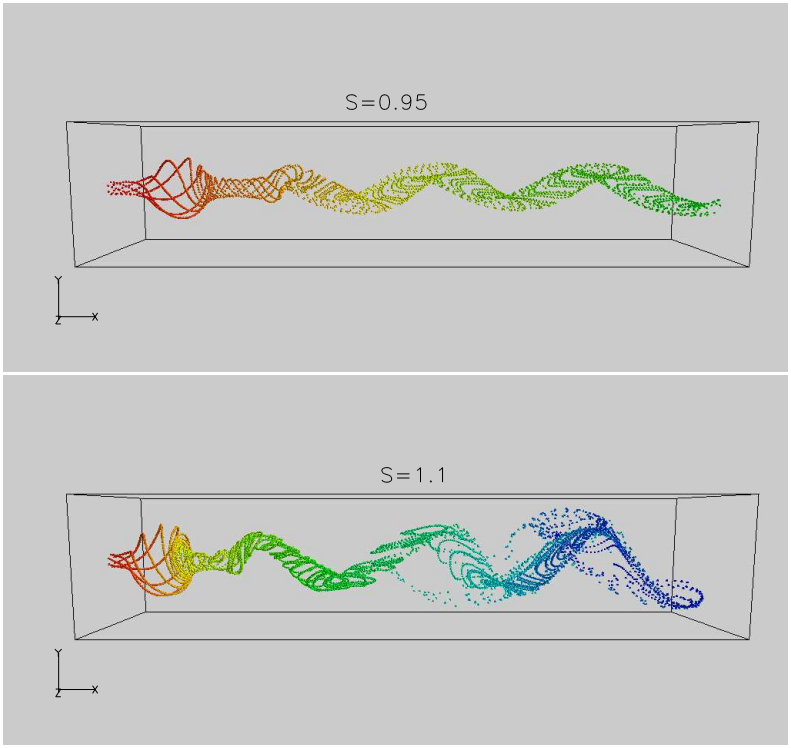

Figure 7: Re=400 case. Streaklines visualization after saturation for different swirl levels. Box size: 20x2x2.

demanding.

The sequence of events is not changed: the breakdown process is still essentially axisymmetric. When the first bubble is formed, the flow behind it accelerates as indicated by the restriction of the streaklines immediately behind the bubble at Time=153. Contemporarily, a new wave starts moving usptream and growing until an other bubble, smaller in size, is formed at Time 210. The formation of the second bubble is again accompanied by acceleration in the wake, and further swelling appears visible behind it. The physical interpretation is the following: an inward motion of the particles moving over the bubble is generated for inertial effects. This increases the angular momentum and reduces the pressure in the wake enhancing the axial acceleration. Although the angular momentum is locally increasing, the strong axial acceleration renders the flow locally supercritical, *i.e.* unable to sustain steady waves of finite wavelength. The second breakdown represents a further transition between two flows dynamically different. This is better seen at Time=310, where the two the swirling flows, ahead and behind the second bubble, are both nearly columnar but appear clearly different.

The three-dimensional instabilities become visible at later stage. In this case the dominant mode is m=2 producing a double helix structure without switching from single to double helix. The period of oscillation is T=3 and the time simulated should be sufficient to observe the a self-sustained mode contaminating the whole domain. Here, however, the perturbation remain localized downstream, behind a specific axial position, and the multiple breakdown structure remains perfectly preserved.

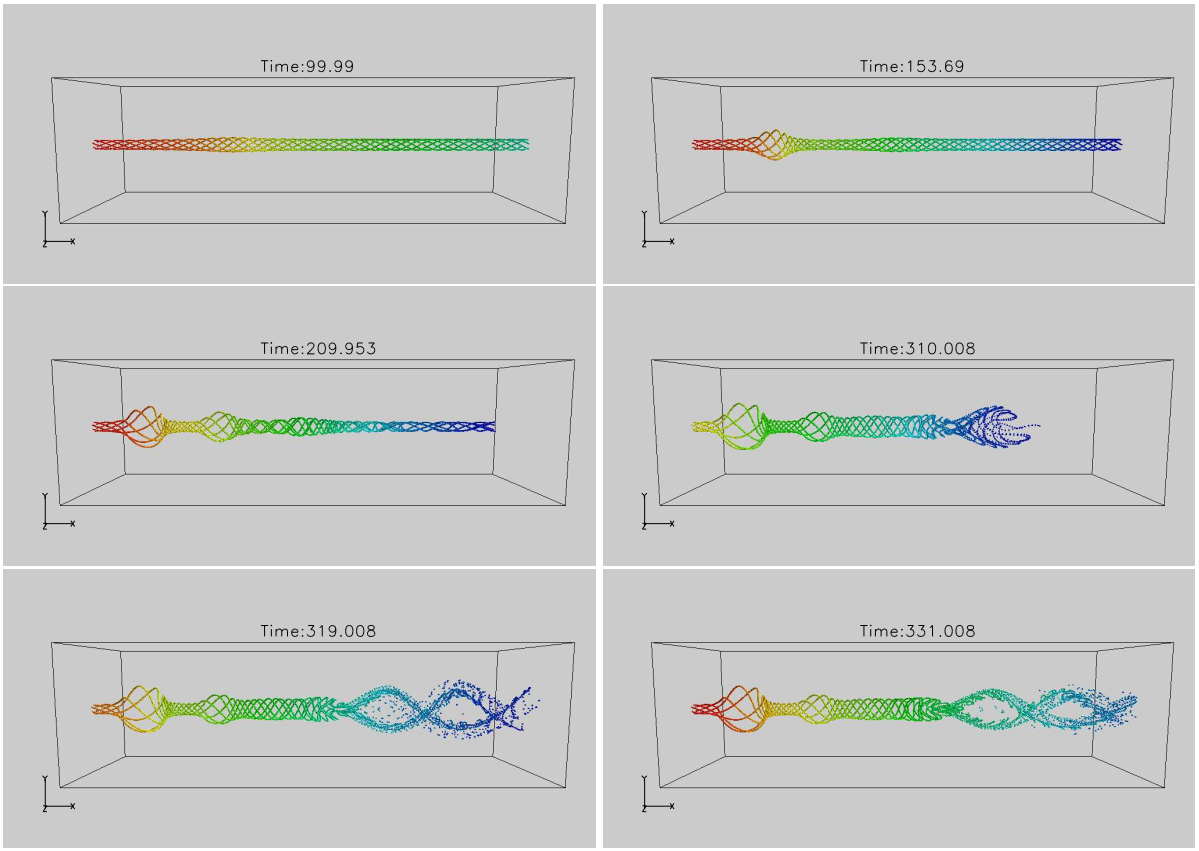

Figure 8: Re=800 S=0.95 case. Temporal evolution of streaklines. Box size: 20x2.8x2.8.

4 Conclusions

A numerical investigation on three-dimensional vortex breakdown in swirling jets has been conducted using Direct Numerical Simulations. The code used is validated against results available in the literature for low Reynolds numbers, and an extension to higher Reynolds number cases is presented.

The numerical computations reveal the main elements underlying the phenomenom: *(a)* large-amplitude axisymmetric waves and *(b)* linear three-dimensional instabilities to azimuthal perturbations. The attempt we have tried to undertake in this paper is to analyze their interactions, or, in other worlds, to see whether the growth of azimuthal modes can interfere with the axisymmetric process of breakdown. It is found that at low Reynolds number a global mode contaminates the entire physical domain and the coupling becomes inportant: the perturbation can penetrate inside the vortex bubble, and the axisymmetric smaller bubbles eventually presented in a multiple breakdown configuration, dissipate as soon as the three-dimensional perturbations become big enough.

At higher Reynolds number, the behaviour is different: a steep transition is generated at some streamwise stations in the wake of the bubbles. A sharp front develops, leaving the peculiar structure of a multiple breakdown substantially unchanged.

REFERENCES

[1] D. Amirante, K.H. Luo. A numerical investigation on vortex breakdown in swirling jets. *IASME Transactions.*, Vol. **7**, 1221-1228, 2005.

[2] B. Benjamin. Theory of the vortex breakdown phenomenon. *J. Fluid Mech.*, Vol. **14**, 593–629, 1962.

[3] F. Grasso, C. Meola. *Handbook of Fluid Mechanics*, Poinsot Ed., 1996.

[4] J.W. Kim, D.J. Lee. Optimized compact finite difference schemes with maximum resolution. *AIAA J.*, Vol. **34**, No. 5, 887–893, 1996.

[5] S. Leibovich. Vortex stability and breakdown: survey and extension. *AIAA J.*, Vol. **22**, No. 9, 1192–1205, 1983.

[6] S. Leibovich. Weakly non-linear waves in rotating fluids. *J. Fluid Mech.*, Vol. **42**, 803–822, 1970.

[7] S.K. Lele. Compact finite difference schemes with spectral like resolution. *J. Comput. Phys.*, Vol. **103**, 16–42, 1992.

[8] H.R. Lewis, P.M. Bellan. Physical constraints on the coefficients of Fourier expansions in cylindrical coordinates. *J. Math. Phys.*, Vol. **31**, 2592–2596, 1990.

[9] T. Loiseleux, J.M. Chomaz and P. Huerre. The effect of swirl on jets and wakes: linear instability of the Rankine vortex with axial flow. *Phys. Fluids.*, Vol. **10**, 1120–1134, 1998.

[10] K. Mohseni, T. Colonius. Numerical treatment of polar coordinate singularities. *J. Comput. Phys..*, Vol. **157**, 787–795, 2000.

[11] P.L. O'Sullivan, K.S. Breuer. Transient growth in circular pipe flow. I. Linear disturbances. *Phys. Fluids.*, Vol. **6**, 3643–3651, 1994.

[12] B. Pier, P.Huerre. Nonlinear self-sustained structures and fronts in spatially developing wake flows. *J. Fluid Mech.*, Vol. **435**, 145–174, 2001.

[13] T.J. Poinsot, S.K.Lele. Boundary conditions for direct numerical simulations of compressible viscous flows. *J Comput. Phys.*, Vol. **101**, 104–129, 1992.

[14] M.R. Ruith, P. Chen, E. Meiburg and T. Maxworthy. Three-dimensional vortex breakdown in swirling jets and wakes: direct numerial simulations. *J. Fluid Mech.*, Vol. **486**, 331–378, 2003.

[15] P.G. Saffman. Vortex dynamics, *Cambridge University Press*, 1992.

[16] T. Sarpkaya. On stationary and travelling vortex breakdown. *J. Fluid Mech.*, Vol. **45**, 545–559, 1971.